Cyanide-orientation distribution by single-crystal NMR of $K(CN)_xBr_{1-x}$

J. H. Walton* and Mark S. Conradi
Department of Physics, Washington University, St. Louis, Missouri 63130
(Received 17 October 1989)

Single crystals of $K(CN)_xBr_{1-x}$ enriched in ^{15}N have been studied by ^{15}N NMR. Because of the anisotropic chemical shift, the NMR frequency spectrum of the orientational glass state reflects the distribution of cyanide orientations. By studying the spectrum at many crystal orientations, the orientation distribution function $P_{(\Omega)}$ has been determined for $x=0.50$ and 0.20. The probability function is largest along [100] directions, intermediate in [110] directions, and nearly zero along [111] axes. The NMR determined $P_{(\Omega)}$ is presented graphically and in terms of the Kubic harmonic functions. The NMR results are in sharp contrast to molecular-dynamics calculations but agree with neutron scattering data for $x=0.53$.

I. INTRODUCTION

Solid solutions of $K(CN)_xBr_{1-x}$ form orientational glasses at low temperatures ($T \lesssim 60$ K) for $x \leq 0.57$. Only the orientations of the CN^- become glassy, with the mass centers retaining long-range order. Because cyanide glass appears to be simple, it has attracted a great deal of attention. However, the unanswered, substantive questions concerning $K(CN)_xBr_{1-x}$ indicate that the system is not so simple.

Pure KCN exists as an orientationally disordered (rotor) cubic crystal from its melt to 168 K (see the phase diagram, Fig. 1).[1-3] At 168 K a first-order phase transition yields an orientationally ordered, orthorhombic structure. In the ordered phase the CN^- are parallel to each other (on time average) and nearly parallel to a previous [110] direction. In different regions, different [110] axes are favored, leading to domain formation and light scattering.[3-6] The two ends of the cyanide are similar (atomic numbers 6 and 7), so head-tail disorder is retained in the ordered structure below 168 K. At 83 K, head-tail (electrical) disorder disappears in a higher-order transition[1,7] into an antiferroelectric state.

The cyanide molecules interact with each other through the lattice, via displacements of the nearby ions, a translation-rotation coupling.[8,9] Direct, through-space interactions are weaker because of the shell of cations separating nearest-neighbor anions. Because of the phonon-mediated interactions and because the phase transition at 168 K involves a long-wavelength distortion, the shear elastic constant C_{44} softens dramatically as the transition is approached from above.[10,11]

Solid solutions $K(CN)_xBr_{1-x}$ can be formed[1] from the mixed melt for arbitrary x. This complete solid miscibility stems from the same crystal structures and similar melting temperatures and lattice parameters of KCN and KBr. For x near unity, decreasing x simply decreases the temperature of the first-order orientational ordering transition (see Fig. 1). This is expected from a mean-field picture, because of the decreasing number of nearest neighbors. Also, as x decreases the entropy change at the transition decreases; by $x=0.57$, the transition entropy has gone smoothly to zero. For $0.57 < x < 1$, there are more than one orientationally ordered phase. Observations of coexisting phases suggest small differences in free energy.[12,13] Many other glass-forming systems share this feature of "competing crystalline phases." With further dilution ($x < 0.57$), continuous freezing occurs as the temperature is lowered. Such a sample exhibits no discontinuities in any measured parameter as a function of temperature. Instead, the CN^- rotate nearly spherically at high temperature, freezing out continuously at lower temperatures.

The nature of the continuous freezing is the central issue concerning orientationally glassy $K(CN)_xBr_{1-x}$. The role of kinetic effects,[14-17] which dominate the freezing of window and polymeric glasses, is not certain. It is not known whether the glass is nonergodic, trapped in a small region of coordinate space. The relative roles of single-particle effects and cooperative effects in the freezing have been compared.[18] A recent theory[19-21] stresses the role of the random, fixed-site selection in generating local, static strains. The magnitude of the strains is larger in related systems with a poorer match of anion sizes,[1,22] such as $K(CN)_xCl_{1-x}$. It should also be pointed

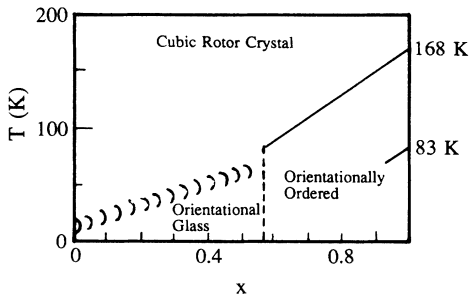

FIG. 1. Phase diagram of $K(CN)_xBr_{1-x}$, from Ref. 1. For $x < 0.57$ the solid solution can be cooled to zero temperature with no transitions. Because the orientational freezing is continuous, the boundaries of the orientational glass region are not well defined. The complicated phase behavior for $x > 0.57$ near the ordering transition has been suppressed, see Refs. 12 and 13.

out that related, nonionic orientational glass systems have been studied: ortho-H_2/para-H_2 (Ref. 23), N_2/Ar (Refs. 24 and 25), and CO/N_2/Ar (Refs. 26 and 27). Electric dipole glasses such as RADP (Ref. 28) and $K_{1-x}Na_xTaO_3$ (Ref. 29) are also related.

In this work we address a simple aspect of the glassy orientational state: in which directions do the cyanide ions point? The orientational probability function $P_{(\Omega)}$ (here Ω is orientation relative to the crystal axes) is determined from single-crystal ^{15}N NMR. $P_{(\Omega)}$ is expected to be sensitive to the interaction potential between the cyanides as well as the cyanide-lattice interactions. Any theory of the freezing in $K(CN)_xBr_{1-x}$ should yield the correct single molecule $P_{(\Omega)}$ before experimentally inaccessible quantities such as neighbor orientational correlations can be reliably predicted.

II. EXPERIMENTAL

Single crystals of $K(CN)_xBr_{1-x}$ were grown from the melt by Matt DeLong at the University of Utah Crystal Growth Laboratory. The starting materials were reagent-grade KBr, KCN purified at Utah, and 99% ^{15}N-enriched KCN. The nominal compositions are $x=0.20$ and 0.50.

The crystals were grown and then machined to right cylinders of ~ 6 mm diameter and ~ 10 mm length. Samples with [100] and [110] cylinder axes were prepared. In all cases, the axes were identified by the natural (100) cleavage planes evident in or on the samples.

The NMR measurements were performed in a 8.0-T superconducting magnet, yielding a 34.5-MHz ^{15}N frequency. The apparatus was cooled using an Oxford Instruments continuous transfer cryostat. The temperature was measured with a Lake Shore carbon-in-glass, calibrated thermometer. The single crystals were held in a glass tube in a goniometer, allowing the samples to be rotated (from the room) about an axis perpendicular to the static magnetic field. With the [110] rotation axis samples, the static field could be aligned along [1$\bar{1}$0], [1$\bar{1}$1], and [001] high-symmetry directions.

The NMR spectrometer is a superheterodyne design. The transmitter output power of ~ 400 W resulted in $\pi/2$ nutation times of about 10 μs. All spectra were obtained from spin echoes, using the $\pi/2_x$-t-π_y-t-echo pulse sequence. For the 17 kHz cyanide linewidths, the available rf field H_1 is barely adequate for clean π pulses. Consequently, composite pulses $(\pi/2_x,\pi_y,\pi/2_x)$ were used in place of π_y pulses.

The cooling scheme employed is one with the sample and rf coil bathed in flowing helium gas. This promotes temperature uniformity, but suffers from rf breakdown when using high-voltage rf pulses. We chose an unusually low L/C ratio to reduce the voltages in the helium gas. The coil was quadfilar (in parallel) and was resonated with many chip capacitors at the low-temperature end. To reduce circulating currents and resulting losses on the rf transmission line, the LC circuit was tapped down for connection to the line. A digital storage oscilloscope was employed to monitor the rf pulses in the LC circuit, to detect breakdown.

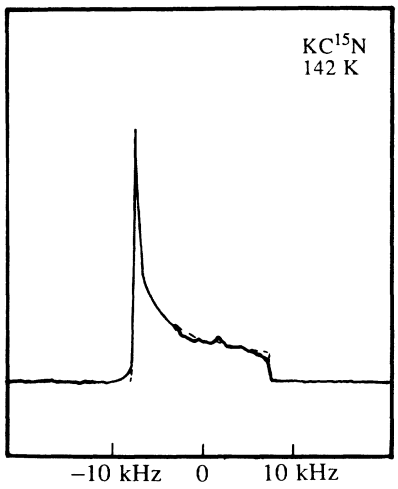

FIG. 2. ^{15}N NMR spectrum at 34.5 MHz of enriched KCN at 142 K in the orientationally ordered phase. The dashed curve is a fit using the theoretical powder pattern, convoluted with a small Gaussian broadening. The good agreement demonstrates that the spectra reported here have little distortion.

The spin echoes were analyzed by shifting the origin of time to the echo peak, phase correcting, exponential time-domain filtering, and then Fourier transforming. We demonstrated to ourselves that reasonable changes in the phasing adjustments yielded only minor shape changes in the spectra.

The line shape for powdered KCN enriched in ^{15}N is shown in Fig. 2. The KCN is orientationally ordered so the spectrum should be the "powder pattern" for uniaxially symmetric chemical shifts.[30] The good agreement between the experimental and predicted spectra demonstrates the lack of distortion of our spectra.

III. RESULTS AND DISCUSSION

Experimental ^{15}N NMR spectra from $K(CN)_xBr_{1-x}$ with $x=0.50$ are shown in Fig. 3. The data were obtained at crystal orientations from 0° to 180° in 10° steps; only some of the results are displayed. In all cases, the 0° orientation has a [100] axis parallel to the static magnetic field. Data from the $x=0.20$ samples are presented similarly in Fig. 4. The experimental spectra do exhibit cubic symmetry: for [100] rotation axes, the α and $90°-\alpha$ line shapes are the same (see the right-hand side of Figs. 3 and 4, $\alpha=20°$ and 70°). For the [110] rotation axes, the α and $180°-\alpha$ line shapes are the same (not shown).

The experiments were performed at 15 K for $x=0.20$ and at 30 K for $x=0.50$. The temperatures are sufficiently low that motional narrowing is not present in the NMR spectra,[31] as demonstrated by the sharpness of the ledge and cusp features in Figs. 3 and 4. Lower temperatures resulted in inconveniently long T_1 values.

An important feature in the spectra is the ledge (step) at the right-hand side (see also Fig. 2). Only molecules that are parallel to the static magnetic field resonate at this extreme frequency. At any other frequency, molecules of many orientations (but all inclined from the field

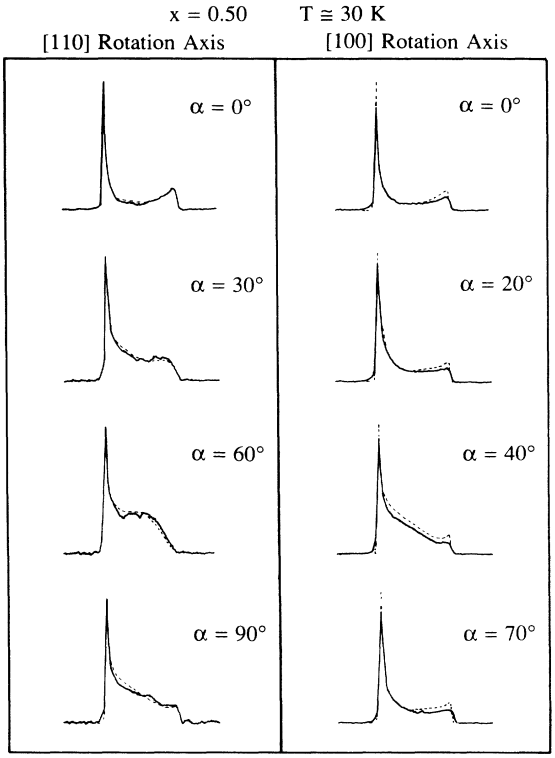

FIG. 3. ^{15}N spectra from single crystals of $K(CN)_xBr_{1-x}$ with $x=0.50$, taken near 30 K. The crystals were rotated about a [110] axis (left) or a [100] axis (right). The rotation angles are marked on each spectrum, with 0° corresponding to the static field oriented parallel to a [001] axis. Thus the left and right 0° spectra are the same orientation, but physically different samples. The [100] 20° and 70° spectra should be the same by symmetry. The dashed curves are fits to the observed line shapes using the coefficients in the first line of Table I.

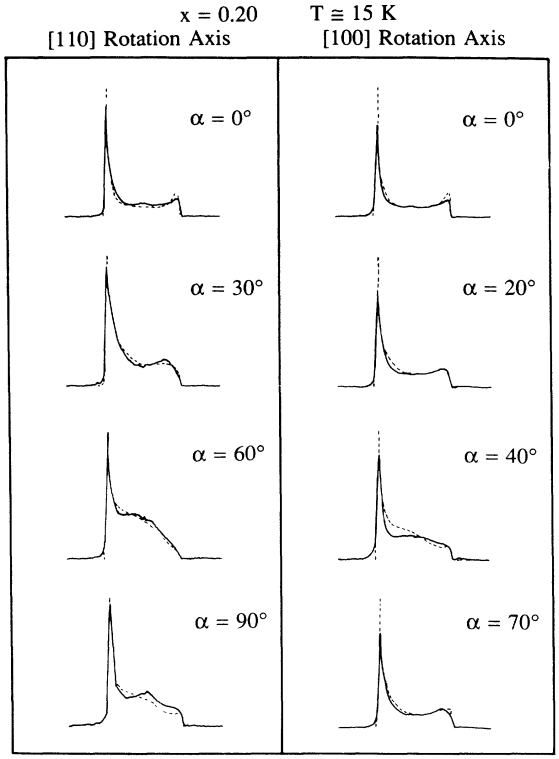

FIG. 4. Same as Fig. 3, but $x=0.20$. The data were taken near 15 K. The coefficients for the dashed fits are from the sixth line of Table I.

by the same angle) contribute intensity as described following. Thus, the amplitude of the ledge (normalized to a fixed integrated area) is proportional to the number of cyanide ions parallel to the field per unit solid angle.

The spectra in Figs. 3 and 4 do change substantially as the samples are rotated in the goniometer. Clearly, $P_{(\Omega)}$ is anisotropic. In particular, the amplitude of the ledge varies, nearly vanishing at 60° with the [110] rotation axis. At this orientation the field is nearly along a [111] direction, giving qualitative evidence that $P_{(\Omega)}$ has deep minima along the [111] directions. However, if one uses only the ledge feature of the spectra, one throws away large amounts of information. We also believe that use of a single spectral feature increases the sensitivity of the physical results to experimental details such as phasing adjustments and the extent of dipole broadening.

We now present the details of the quantitative analysis of the spectra in Figs. 3 and 4 (and the intermediate angles not displayed). The ^{15}N spin in a cyanide ion experiences an uniaxially symmetric, anisotropic chemical shift. That is, the NMR frequency ω varies according to[30]

$$\omega=\omega_0+\omega_0\Delta\sigma(\cos^2\phi-\tfrac{1}{3}) . \quad (1)$$

Here ϕ is the angle between the cyanide axis and the static magnetic field, ω_0 is the isotropic or liquid average frequency, and $\Delta\sigma$ is the shift anisotropy, approximately 490 ppm for ^{15}N in cyanide (see Fig. 2). The ledge at the right corresponds to $\phi=0$ (a unique direction), and the cusp at the left is $\phi=90°$. The simplicity of the relationship (1) between NMR frequency and cyanide orientation makes the interpretation of the spectra in terms of $P_{(\Omega)}$ direct and unambiguous.

We numerically calculated the NMR line shape $I_{(\omega)}$ resulting from an assumed probability distribution $P_{(\Omega)}$. The cyanide orientations Ω relative to the crystal axes were sampled on a grid (typically 2.5° in azimuth and 2.5° in polar angle; finer grids did not change the line shape). At each orientation, the NMR frequency was computed from Eq. (1) for a given external field orientation. A Δ function at the NMR frequency was then contributed to the composite spectrum $I_{(\omega)}$. The area of the Δ function was proportional to the product of $P_{(\Omega)}$ and the solid angle "belonging" to the particular orientation Ω on the sampling grid. Finally, a modest Gaussian broadening was applied by convolution to treat the effects of dipolar interactions.

The orientation probability function $P_{(\Omega)}$ is expected to have cubic symmetry in the $K(CN)_xBr_{1-x}$ system for $x<0.57$. This is true whether the system is truly a cubic orientational glass or forms microscopic orientationally ordered domains.[32,33] As mentioned previously, our spectra always show the cubic symmetry. In terms of $P_{(\Omega)}=P_{(x,y,z)}$ with x,y,z on the unit sphere, P must be invariant under any interchanges and/or sign changes of

TABLE I. Kubic harmonic coefficients.

CN concentration x	Source	a_0	a_4	a_6	a_8	a_{10}
0.50	NMR[a,b]	1.0	0.62	−0.16	0.10	−0.13
0.50	NMR	1.0	0.58	−0.12	0.21	
0.50	NMR[b]	1.0	0.54	−0.06		
0.53	neutron[b,c]	1.0	0.36	−0.08		
0.50	MD[d]	1.0	−0.70	0.52		
0.20	NMR[a,b]	1.0	0.54	−0.01	0.23	
0.20	NMR[b]	1.0	0.49	−0.01		
0.25	MD[d]	1.0	−0.80	0.75		

[a] These coefficients used for dashed curves in Figs. 3 and 4.
[b] These coefficients used in Fig. 5.
[c] Neutron diffraction at 10 K, Ref. 36.
[d] Molecular dynamics, Ref. 40; low-temperature (20 K) values listed.

x,y,z. It is convenient to write $P_{(\Omega)}$ as an expansion in the Kubic harmonics,[34]

$$P_{(\Omega)}=P_{(x,y,z)}=\sum_n a_n K_{n(x,y,z)} . \tag{2}$$

The first few Kubic harmonic functions are

$$\begin{aligned}
K_0&=1 ,\\
K_4&=\{5[(3)(7)]^{1/2}/4\}(x^4+y^4+z^4-\tfrac{3}{5}) ,\\
K_6&=\{3(7)11[(2)(13)]^{1/2}/8\}(x^2y^2z^2+[K_4]/22-\tfrac{1}{105}) ,\\
K_8&=\{(5)13[3(11)17]^{1/2}/16\}\\
&\quad\times(x^8+y^8+z^8-28[K_6]/5-210[K_4]/143-\tfrac{1}{3}) ,\\
K_{10}&=(667.60)(x^{10}+y^{10}+z^{10}-2.380[K_8]\\
&\quad-7.415[K_6]-1.469[K_4]-0.2727) .
\end{aligned} \tag{3}$$

The symbol $[K_n]$ means the function K_n without the normalization prefactor. By symmetry, only even values of n appear. There is no K_2 function, because $x^2+y^2+z^2=1$. A correction to the original[34] form of K_8 is listed.[35] We derived the K_{10} function by starting with $x^{10}+y^{10}+z^{10}$ and then numerically implementing the Gram-Schmidt procedure to make the function orthonormal to K_0, K_4, K_6, and K_8. The coefficients in Eq. (2) are restricted by the requirement that P be non-negative for all x,y,z.

The coefficients in Eq. (2) that fit the experimental spectra are listed in Table I. For $x=0.50$, the first three lines in Table I differ only in the highest Kubic harmonic included in the fit (6, 8, or 10). Similarly, the sixth and seventh lines are for $x=0.20$ and differ in the number of terms in the expansion (2). In Figs. 3 and 4 the experimental spectra are solid curves. The fits to the data appear as dashed curves and come from the first and sixth lines of Table I. The computed spectra reproduce most of the features of the experimental spectra. The largest deviations are for the $x=0.20$ sample with the field near a [110] direction (90° for [110] rotation axis and 45° for [100] rotation axis).

The heights of the cusp features of the calculated spectra are very sensitive to the magnitude of the broadening applied. The actual dipolar broadening may be anisotropic. Thus, we ignored the cusp feature in determining the coefficients of best fit.

Although the coefficients in Table I change upon inclusion of the eight- and tenth-order terms, the function $P_{(\Omega)}$ changes little. This is demonstrated in Fig. 5, where polar representations of $P_{(\Omega)}$ in the (100) and (110) planes appear. Some differences between the solid and dashed curves are evident, but the main features are the same. The physical conclusions do not depend on the details of the fitting procedure.

Neutron diffraction[36] on $x=0.53$ material was interpreted to yield $P_{(\Omega)}$ in terms of the coefficients in the fourth line of Table I. In the polar plots of Fig. 5, the neutron scattering $P_{(\Omega)}$ appears as a dotted curve. It is clear that the neutron results for $x=0.53$ and the ^{15}N NMR results for $x=0.50$ are in substantial agreement. It should be pointed out that a brief report[37] of a neutron scattering study claims that the cyanides in $x\sim0.20$ material are oriented predominantly along [111], in contrast with the $x=0.20$ data in Fig. 5.

Elschner and Petersson[38] examined the related system $Na(CN)_xCl_{1-x}$ with ^{23}Na NMR, the sodium serving as an indirect probe of cyanide orientations. They found electric field gradients at the sodium sites with [100] principal axes. They argue that this can only occur for cyanides oriented primarily in [100] directions, such as found here in $K(CN)_xBr_{1-x}$ (see Fig. 5). No quantitative measure of the extent of alignment was given.

Molecular dynamic simulations[39,40] have been reported for $K(CN)_xBr_{1-x}$. The potential parameters were tuned[41] to yield agreement with the experimental phase diagram. The authors report preferential alignment along and near [111] axes in the orientational glass state for $x=0.50$ and 0.25. This is in striking contrast to the NMR and neutron results displayed in Fig. 5. The simulation values[40] of the fourth- and sixth-order coefficients at the lowest temperatures are listed in Table I (lowest line for each concentration). The signs are opposite to the coefficients from NMR and neutron diffraction.

The discrepancy between the experiments and the molecular dynamic simulations is substantial. It may be that the simulations used incorrect interaction potentials or that the simulated systems are too small. More importantly, the time scales are vastly different: experimental samples are cooled to low temperatures over ~1 h, while

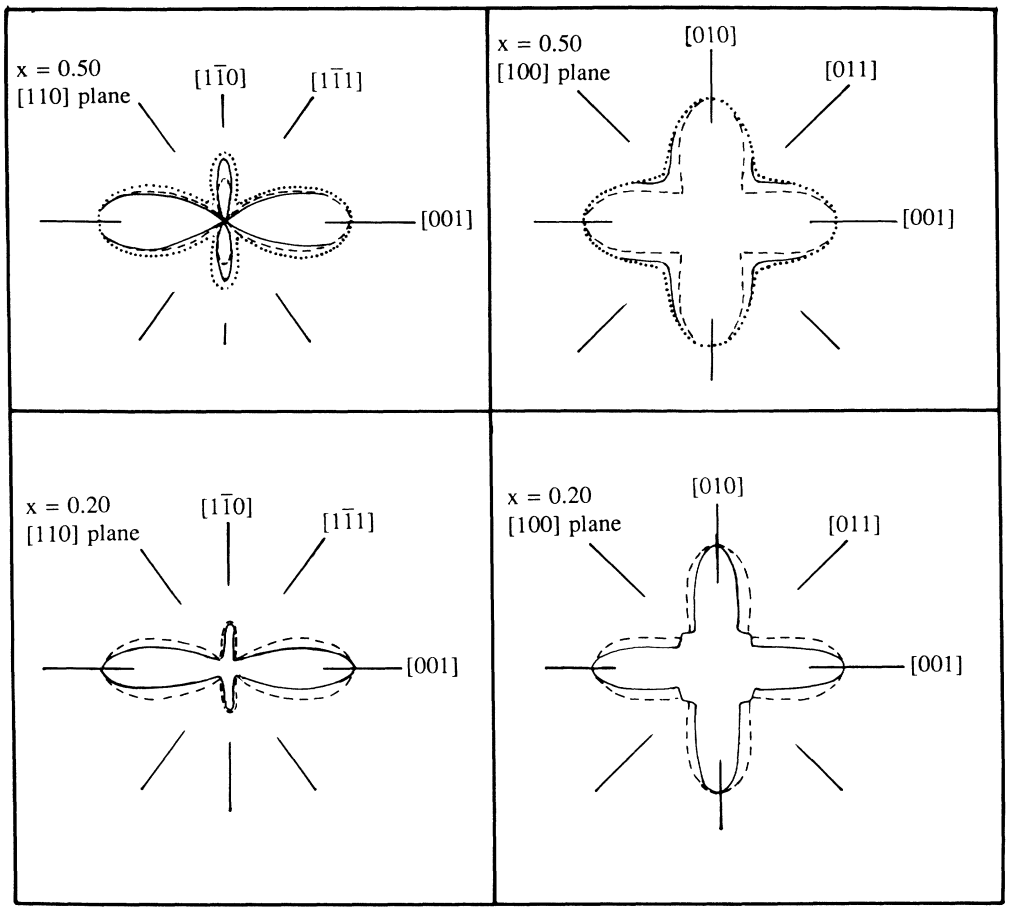

FIG. 5. Polar representation of the orientation probability distribution function $P_{(\Omega)}$; cuts along two planes are shown. The solid curves correspond to the first set of Kubic harmonic coefficients for each concentration in Table I. The dashed curves for $x=0.50$ are from the third line in Table I. The dashed curves for $x=0.20$ are from the seventh line of Table I. The dotted curves in the upper figures are from neutron diffraction with $x=0.53$, Ref. 36.

the calculations simulate a time of order 10^{-11} s. In a glassy system, short times may be inadequate for obtaining the experimental ground state. In any event, the molecular-dynamics simulations produce single-particle orientation distributions that are qualitatively different from the observations. The simulations can "measure" properties (e.g., two-molecule orientation correlations) that are inaccessible by experiments. Thus, it is very important to compare the simulations with experiments, when available.

IV. CONCLUSIONS

The orientation probability distribution function $P_{(\Omega)}$ of cyanide ions in $K(CN)_xBr_{1-x}$ has been determined by ^{15}N NMR in single crystals. Because of the anisotropy of the ^{15}N chemical shift, the NMR frequency depends on the cyanide orientation to the external field. The spectra at several crystal orientations result in a direct and unambiguous determination of $P_{(\Omega)}$. At the low temperatures and the concentrations ($x=0.20$ and 0.50) used, the cyanide orientations are frozen out, forming an orientational glass. The probability $P_{(\Omega)}$ has a large anisotropy; the maxima are along [100] directions and deep minima occur along the [111] axes. The function $P_{(\Omega)}$ exhibits cubic symmetry, as expected. The orientation distributions for $x=0.20$ and $x=0.50$ are similar, suggesting the importance of single particlelike terms in the effective potential. The present NMR results are in agreement with the $P_{(\Omega)}$ determined by neutron diffraction for $x=0.53$. Both results disagree with molecular dynamics simulations that find strong [111] preferential alignment.

ACKNOWLEDGMENTS

This research was funded in part through National Science Foundation (NSF) Grant No. DMR 87-02847 and in part through the generosity of the donors to the Petroleum Research Fund, administered by the American Chemical Society. We appreciate helpful conversations with J. M. Rowe and L. J. Lewis. L. J. Lewis and M. L. Klein kindly sent us early versions of their manuscripts.

*Now at Naval Research Lab., Code 6126, Washington, D.C. 20375.

[1]F. Luty, in *Proceedings of International Conference on Defects in Insulating Crystals, Riga,* edited by V. M. Turkevich and K. D. Schwartz (Springer-Verlag, Berlin, 1981).

[2]L. J. Lewis and M. L. Klein, Phys. Rev. Lett. **59**, 1837 (1987).

[3]D. Durand, L. C. S. do Carmo, A. Anderson, and F. Luty, Phys. Rev. B **22**, 4005 (1980).

[4]M. D. Julian and F. Luty, Phys. Rev. B **21**, 1647 (1980).

[5]A. Tzalmona and D. C. Ailion, Phys. Rev. Lett. **44**, 460 (1980).

[6]W. Buchheit, S. Elschner, H. D. Maier, J. Petersson, and E. Schneider, Solid State Commun. **38**, 665 (1981).

[7]B. Koiller, M. A. Davidovich, L. C. S. do Carmo, and F. Luty, Phys. Rev. B **29**, 3586 (1984).

[8]M. L. Klein and I. R. McDonald, Chem. Phys. Lett. **78**, 383 (1981); K. H. Michel and J. Naudts, Phys. Rev. Lett. **39**, 212 (1977).

[9]D. Sahu and S. D. Mahanti, Phys. Rev. B **26**, 2981 (1982).

[10]J. Z. Kwiecien, R. C. Leung, and C. W. Garland, Phys. Rev. B **23**, 4419 (1981).

[11]C. W. Garland, J. Z. Kwiecien, and J. C. Damien, Phys. Rev. B **25**, 5818 (1982).

[12]J. M. Rowe, J. J. Rush, and S. Susman, Phys. Rev. B **28**, 3506 (1983).

[13]K. Knorr and A. Loidl, Phys. Rev. B **31**, 5387 (1985).

[14]A. Loidl, R. Feile, and K. Knorr, Phys. Rev. Lett. **48**, 1263 (1982).

[15]S. Bhattacharya, S. R. Nagel, L. Fleishman, and S. Susman, Phys. Rev. Lett. **48**, 1267 (1982).

[16]J. M. Rowe, J. J. Rush, D. G. Hinks, and S. Susman, Phys. Rev. Lett. **43**, 1158 (1979).

[17]K. H. Michel and J. M. Rowe, Phys. Rev. B **22**, 1417 (1980).

[18]A. Loidl, T. Schrader, R. Bohmer, K. Knorr, J. K. Kjems, and R. Born, Phys. Rev. B **34**, 1238 (1986).

[19]K. H. Michel, Phys. Rev. Lett. **57**, 2188 (1986).

[20]K. H. Michel, Phys. Rev. B **35**, 1405 (1987).

[21]K. H. Michel, Phys. Rev. B **35**, 1414 (1987).

[22]E. C. Garcia, K. Knorr, A. Loidl, and S. Haussuhl, Phys. Rev. B **36**, 8517 (1987).

[23]A. B. Harris and H. Meyer, Can. J. Phys. **63**, 3 (1985).

[24]N. S. Sullivan, C. M. Edwards, and J. R. Brookeman, Mol. Cryst. Liq. Cryst. **139**, 365 (1986).

[25]W. Press, B. Janik, and H. Grimm, Z. Phys. B **49**, 9 (1982); H. Klee, H. O. Carmesin, and K. Knorr, Phys. Rev. Lett. **61**, 1855 (1988).

[26]J. H. Walton, M.-C. Wu, and M. S. Conradi, Can. J. Chem. **66**, 680 (1988).

[27]S.-B. Liu and M. S. Conradi, Solid State Commun. **49**, 177 (1984).

[28]E. Courtens, Helv. Phys. Acta **56**, 705 (1983).

[29]M. Maglione, U. T. Hochli, and J. Joffrin, Phys. Rev. Lett. **57**, 436 (1986).

[30]A. Abragam, *The Principles of Nuclear Magnetism* (Clarendon, Oxford, 1961).

[31]M. A. Doverspike, M.-C. Wu, and M. S. Conradi, Phys. Rev. Lett. **56**, 2284 (1986).

[32]J. Ihm, Phys. Rev. B **31**, 1674 (1985).

[33]K. Knorr, E. Civera-Garcia, and A. Loidl, Phys. Rev. B **35**, 4998 (1987).

[34]F. C. Von der Lage and H. A. Bethe, Phys. Rev. **71**, 612 (1947).

[35]R. S. Seymour and A. W. Pryor, Acta Cryst. **B26**, 1487 (1970).

[36]A. Loidl, K. Knorr, J. M. Rowe, and G. J. McIntyre, Phys. Rev. B **37**, 389 (1988).

[37]P. Wochner, E. Burkel, J. Peisl, C. M. E. Zeyen, and W. Petry, in *ILL Workshop on Dynamics of Disordered Materials* (Springer-Verlag, Berlin, in press).

[38]S. Elschner and J. Petersson, J. Phys. C **19**, 3373 (1986).

[39]L. J. Lewis and M. L. Klein, J. Phys. Chem. **91**, 4990 (1987).

[40]L. J. Lewis and M. L. Klein, Phys. Rev. B **40**, 7080 (1989).

[41]L. J. Lewis and M. L. Klein, Phys. Rev. B **40**, 4877 (1989).